Thin Solid Films 517 (2009) 6264–6270

Contents lists available at ScienceDirect

Thin Solid Films

journal homepage: www.elsevier.com/locate/tsf

X-ray textural and microstructural characterisations by using the Combined Analysis Approach for the optical optimisation of micro- and nano-structured thin films

M. Morales [a,*], D. Chateigner [b], L. Lutterotti [c]

[a] CIMAP (ex-SIFCOM) – ENSICAEN, CNRS, CEA, Université de Caen Basse-Normandie, 6 Bd du Marechal Juin, 14050 Caen Cedex 04, France
[b] CRISMAT-ENSICAEN, CNRS, Université de Caen Basse-Normandie, 6 Bd du Marechal Juin, 14050 Caen Cedex 04, France
[c] Dipartimento di Ingegneria dei Materiali, Universita di Trento, 38050 Trento, Italy

ARTICLE INFO

Available online 25 February 2009

Keywords:
Semiconductors
Nanostructures
Structural properties
Texture
X-ray diffraction
Sputtering

ABSTRACT

Nano/micro-crystalline silicon, silicon carbide and zinc selenide sputtered films are chosen to illustrate the potentialities of the X-ray Combined Analysis methodology in characterising textures, structures, residual stresses, phase amounts, twin faults, layer thicknesses and crystallite sizes and shapes. The observed textures range from weak (in Si and SiC films) to very strong (in ZnSe). In all films, crystallites are found anisotropic in shapes and sizes. In nc-Si, no residual stress is observed, but the cell parameters deviate from bulk values due to crystal size reduction. The layer thickness as probed by X-ray diffraction imposes films porosities. In unstressed SiC films the two polymorph phases (hexagonal and cubic) are present and both are textured. In ZnSe films, a ratio of around 55/45 for the cubic and hexagonal phases respectively is quantified and large tensile in-plane residual stresses reaching several hundreds of MPa calculated.

1. Introduction

Thin film X-ray analysis is nowadays more and more confronted with major problems when the elaborated films exhibit desired or not preferred orientations. Indeed the intensity variations of the X-ray reflections are dependent simultaneously on the texture and the structure, and the texture is *a priori* unknown. This makes indispensable a quantitative texture analysis (QTA) in order to interpret correctly the diffraction diagrams in terms of structure analysis (and this latter can deviate considerably from the bulk material). In turn, without an exact knowledge of the structure, the quantitative texture determination is for the less delicate to operate. All these difficulties are emphasized also when (i) the films are nanostructured, (ii) exhibit a lot of inter- and intra-phases peak overlaps and (iii) when the samples are composed of several layers of different crystallised phases with *a priori* different textures. Volume and absorption corrections become then necessary, which are not operated the same on a covered layer, top film, substrate.., and which bias structural and textural approaches. Finally, texture, structure … determinations remain furthermore depending on the microstructural states, like crystalline defects (point, linear, planar or volumic), composition variations, microstrains and/or residual stresses. For instance, stacking faults or/and finite and anisotropic crystallite sizes or/and residual stresses will make inter- and intra-phase overlaps varying with hkℓ and sample orientations, which in turn will be quantitatively determined only if the other parameters are known satisfactorily.

A new methodology called "Combined Analysis" [1] has been recently developed and implemented in the MAUD software [2] in order to determine as much as possible parameters accessible using ray scattering, in the goal of optimising films properties. This technique is based on cyclic refinements of the diffraction diagrams measured for different sample orientations and by using the Rietveld Method [3]. The texture is then modelled through the refinement of the Orientation Distribution Function (ODF) of crystallites using whichever implemented formalism (General spherical harmonics, WIMV, E-WIMV, components [4]…), the anisotropic crystallite sizes, shapes and microstrains using the Popa formalism [5] and the residual stresses through the film elastic constants refinement from the ODF and single crystal tensors using Voigt, Reuss, Hill or geometric mean approaches [6]. The film thicknesses can also be refined by using the absorption corrections [7]. In this program, a first Rietveld refinement is operated in a cyclic manner on sets of diffraction diagrams measured for as many as necessary sample orientations, Le Bail-extracted intensities then serve a first QTA cycle, the result of which serving to correct diagrams for the next Rietveld cycle... If residual stresses are present, the macroscopic elastic tensors are calculated after the ODF refinement in order to correct for diffraction peak positions. The operation leads to the determination of the parameters satisfying the best solution of the whole ensemble of measurements.

In this paper we illustrate the use of this combined approach in the aim of optimising optical properties of micro- and nano-crystallised (nc) thin films deposited by magnetron sputtering: (i) nc-Si crystallites embedded in an amorphous SiO_2 matrix and deposited on silica glass and [100]-Si single crystal substrates, for which texture, film thicknesses and anisotropic Si crystallite sizes determination are

* Corresponding author. Tel.: +33 2 31 45 26 58; fax: +33 2 31 45 26 60.
E-mail address: magali.morales@ensicaen.fr (M. Morales).

0040-6090/$ – see front matter © 2009 Elsevier B.V. All rights reserved.
doi:10.1016/j.tsf.2009.02.104

coupled; (ii) nc-SiC crystallites embedded in an amorphous SiC matrix and deposited on glass and [100]-Si single crystal substrates, as an example of combined determination of texture, anisotropic SiC nanosizes and phase percentage of the two SiC polytypes; (iii) Cr^{2+}:ZnSe thin films deposited on silica glass substrates to illustrate the combined determination of texture-structure-phase amounts-crystallite sizes, in the presence of both residual stresses and twin faults.

2. Experimental details

This methodology requires that datasets are measured in as many sample orientations as necessary for a good ODF determination, *i.e.* around 1000 2θ-scans given a reasonable grid resolution of 5°×5° for that kind of films. Such a number of diffraction patterns to acquire would already be unrealistic using point detectors. In this work we used a Huber 4-circles X-ray diffractometer at the average Cu K_α radiation ($\lambda_{Cu}=1.5418$) equipped with a curved position sensitive detector (INEL CPS 120) [8], which spans a 120° range in 2θ, allowing the simultaneous recording of several pole figures and the full diffraction diagram. These latter were measured for tilt (χ) and azimuth (φ) angles in the 0–60° and 0–355° ranges respectively, both using 5° steps. The instrumental resolution function was determined by a full mapping (in ω, χ and 2θ ranges) of the diffractometer space using the NIST LaB_6 powder standard used for the International Crystallographic round-robin. Preferred orientations are expressed in orientation density units, *i.e.* multiples of a random distribution (m.r.d.). The Si [9], SiC [10] and Cr^{2+}:ZnSe [11] films investigated here were grown by reactive magnetron sputtering as described in previous works. We complemented our Combined Analysis characterisation by High Resolution Transmission Electron Microscopy (HRTEM) on films cross-sections using a Topcon 002B microscope.

3. Results and discussion

3.1. nc-Si films: texture, anisotropic crystallite shapes, cell parameters and thickness determination

Nanocrystalline silicon (nc-Si) thin films are promising structures for a wide range of applications in micro- and opto-electronics [12]. In such films a deposition temperature lowering is required in order to enable the use of low cost substrates and to benefit of the peculiar optical phenomena accompanying crystal sizes reduction, and still remained the main challenge for large area microelectronic applications. We choose to deposit nc-Si films by the reactive magnetron sputtering technique on [100]-Si single crystals and silica glass (a-SiO_2) substrates. As the films growth and crystallization mechanisms strongly influence their resulting refractive indices, *via* crystallite sizes and crystalline phase amounts modifications in the films, a detailed structural and microstructural characterisation of the films is required. For silicon the most intense diffraction lines are 111, 220 and 311, and we then measured X-ray diffraction patterns with an incident angle corresponding to the Bragg angle of the 111 reflection ($\omega=14.2°$). Such patterns reveal that the films are made of nanocrystalline silicon with multiple texture components and anisotropic crystallite shapes (Fig. 1). When a textured film exhibit anisotropic crystallite shape, if the texture information is not used (*e.g.* when it is impossible as in random powders or when the textured sample as been measured with too few orientations), the anisotropic shape of the crystallites can be, at least partially, masked. Indeed for one measured orientation the crystallite sizes are only estimated from some {*hkl*} planes preferentially brought to diffraction while the others are not detected, resulting in a systematic lowering of the shape anisotropy. For the case of a textured sample having (111) planes mostly parallel to the sample surface and [111] elongated crystallites perpendicular to it, the long dimension of the crystallites is more favoured than the short one, and this latter has to be probed with other *hkl* lines. However, the long dimension is still underestimated if low ω values are used, because this configuration does not ensure to probe the maximum of the distribution of the crystallites orientation. Such biased estimations are often encountered in works reporting silicon crystallite size determination using the Scherrer formula, resulting in overestimated sizes with underestimated shape anisotropy [13–15]. The integral width approach used by Houben et al. [16] or even the direct Fourier deconvolution of the signal from the X-ray profile [17] gives results closer to the reality but are still however lowering the shape anisotropy.

To overcome the above-mentioned problems, the use of the combined approach is required with the simultaneous analysis of the anisotropic shape using the Popa formalism based on the symmetrised spherical harmonics and the quantitative texture using the WIMV approach. This allows one to obtain a better estimate of the anisotropic shapes, weighted by the volumic ratio of material in a given orientation and gives very satisfactory fits (Fig. 1) with structural reliability factors R_B, R_w and R_{exp} around 5% and texture reliability factors RP_0 [18] generally in the 1–3% range. Such reliabilities, if they could be achieved by simple texture parameter fits like used in the March–Dollase [19] or Lotgering [20] approaches, would not correspond to a physically understandable model of the texture in our case, because of the fairly complex ODF of our films, as is seen on the inverse pole figure (Fig. 2(a)). Indeed multiple preferred orientations are observed with texture strengths around 2 to 3 times a random distribution, with a tendency to achieve lower strengths for films grown on a-SiO_2 substrates. The texture components are evolving with the substrate to target distance, with <110> and <hhl> (l larger than 2) orientations favoured for smaller and larger distances respectively. For all the studied films, no perfect <111> orientation is observed whereas a systematic elongation of the anisotropic Si crystallites along one [111] direction is present. Fig. 2(b) illustrates the mean anisotropic shape as refined using the Combined Analysis that coincides perfectly with high resolution TEM microscopy images (Fig. 2(c)) in which elongated single Si nanocrystals embedded in an amorphous SiO_2 matrix are evidenced. As schematically illustrated in Fig. 2(b), the average crystallite size along [111] is around 9–10 nm which is around four times less than the value estimated by the Scherrer formula, and 2–4 nm in the perpendicular directions. The crystal shape anisotropy is therefore much larger than the one deduced from single pattern analysis. The film structure is free of stress and microstrain, and the unit-cell of the silicon nanopowders is always larger than for bulk silicon. In given conditions, both the target to substrate distance and the substrate nature control the crystalline fraction of the films as well as their structural, textural and microstructural

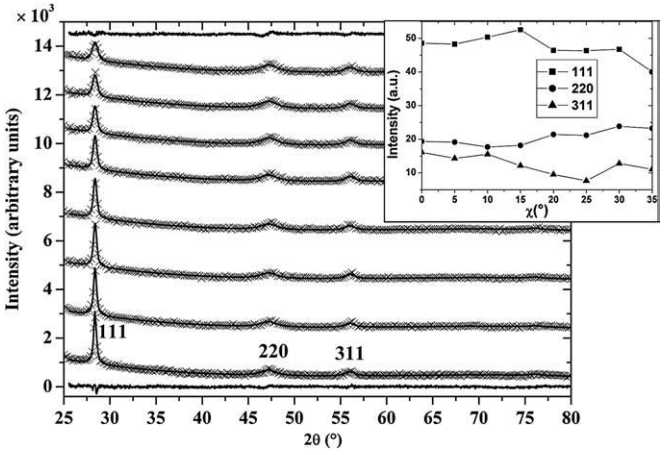

Fig. 1. Experimental (×) and fitted (line) 2θ patterns for selected χ-orientations of one nc-Si/a-SiO_2 sample. Large peaks (small crystallites) are observed and the presence of texture is evidenced by peak intensity variations with χ (inset). Bottom pattern: $\chi=0°$; top pattern: $\chi=35°$; $\Delta\chi=5°$. Differences between measured and calculated diagrams are shown for the bottom and top patterns and illustrate the fit quality.

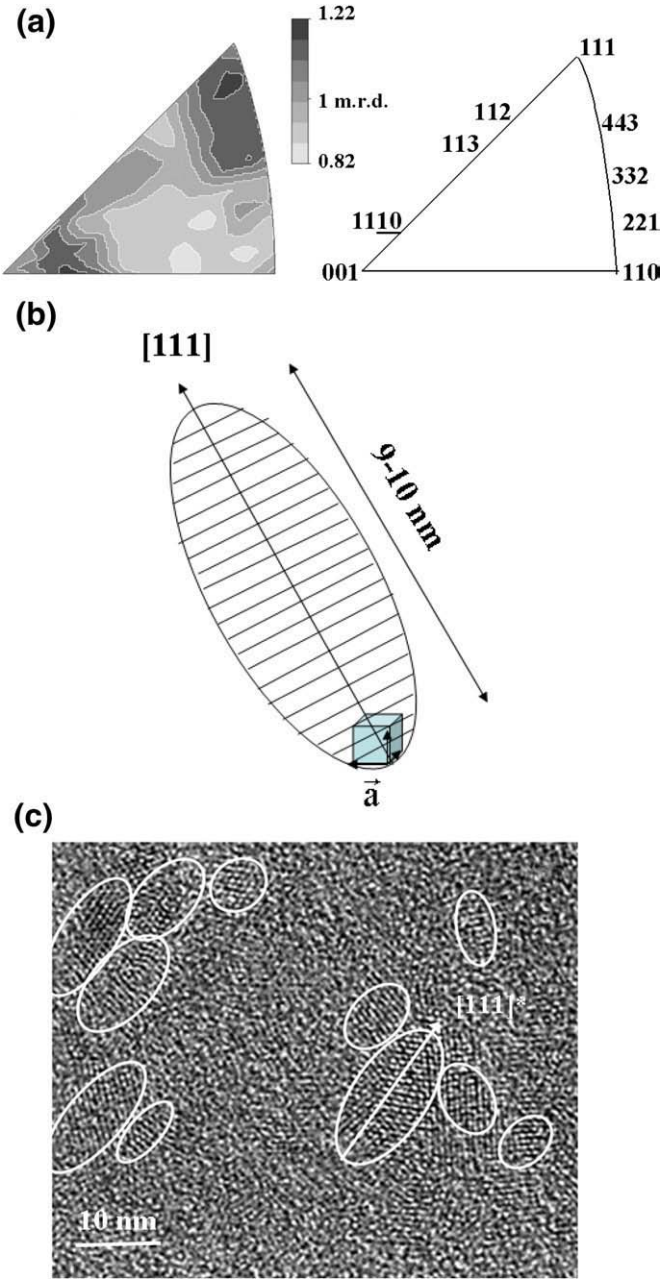

Fig. 2. (a) Inverse pole figure (left) for the normal direction of the Si thin film of Fig. 1, and calculated from the refined ODF and the corresponding pole locations (right) are indicated by their Miller indices (linear density scale, equal area projection); (b) schematic representation of the refined mean crystallite shape and (c) HRTEM image of elongated Si nanocrystallites.

features. Furthermore, the procedure enables to refine the film thickness from the large angle part of the data, and since the films thickness are "seen" under various incidences due to the χ rotation of the texture scans. Such thicknesses are the ones as probed by X-rays, *i.e.* if strong porosity is present the X-ray thickness appears smaller. This is evidenced on nc-Si thin films deposited on a-SiO_2 substrate for different inter-electrode distance (Table 1) and for which the porosity has been measured by X-ray reflectivity [9]. While profilometry indicates the full geometrical thickness of the films, X-ray refinements measure their effective thickness, the difference between the two approaches highlighting film porosities as evidenced also in the cross-sectional TEM images.

The optical properties of the nc-Si films (refractive index and Tauc gap values) are strongly correlated to their microstructural properties [9], particularly to the nanocrystal sizes and to their porosity (presence of numerous microcavities), showing that some nc-Si thin film structures can be envisaged for example for the realisation of microelectronic transistors.

3.2. Polytyped nanocrystalline SiC films: texture, anisotropic crystallite shapes, cell parameters, phase percentage and thickness determination

For the development of a great variety of microelectronic and optoelectronic devices such as bipolar transistors, photodetectors and electroluminescent diodes, silicon carbide still remains the material of choice among the available CMOS-integrated semiconductors [21]. In order to achieve low-temperature growth of high quality crystallized SiC, we investigated using X-ray analyses nc-SiC films deposited on a-SiO_2 or [100]-Si single crystal substrates at various deposition temperatures T_d in the 200–600 °C range. As previously seen for nc-Si films, for T_d>200 °C the nc-SiC film exhibit fibre-like texture components. The X-ray diagrams (Fig. 3(a)) measured for $\omega = 17.1°$, Bragg angle of the 111 reflection of cubic SiC, can be indexed in an apparent cubic cell of the polytype 3C-SiC (F-43m space group). These diagrams exhibit also strong and anisotropic broadening of the diffracted lines due to the anisotropic shape of the SiC crystallites. Upon decreasing T_d, the intensity of all the diffraction lines is lowered, indicating that the corresponding films are less and less crystallised or the growing crystallites are smaller and smaller [10]. The relatively large width of the diffraction lines, indicative of the presence of very small SiC crystallites, cannot exclude a priori the presence of other polytypes such as the hexagonal 6H-SiC ($P6_3mc$ space group) most commonly observed, and that can derive from 3C-SiC via stacking faults occurring during the growth. In particular, the peak shoulder at $2\theta \approx 35°$ cannot be indexed in the 3C-SiC cubic cell (Fig. 3(a)). In order to overcome all these problems (strong peak overlaps, two textured phases and anisotropic sizes), we use the Combined Analysis Approach and in a first step, for the refinement of the XRD spectra, we considered only the 3C-SiC phase with preferential orientations and with anisotropic crystallite shapes. However, the discrepancies between the calculated and the experimental diagrams suggest the presence of another phase in the films, discrepancies more marked when T_d decreases. The 6H-SiC textured polytype was therefore subsequently introduced with a proportion used as refinement fitting parameter and with isotropic crystallite sizes. With these parameters, a good agreement between experimental and calculated spectra (Fig. 3(a)) is found for specific proportions of 6H-SiC, with respectively Rietveld and texture reliability factors not exceeding 5.2% and 1.4% respectively. The refined a-cell parameter of the 3C-SiC phase (Table 2) is around 4.38 Å whatever the T_d values, while the a- and c-cell parameters for 6H-SiC are refined to around 3.09 Å and 15.25 Å, respectively. These values are always larger than those for the counterparts bulk SiC polytypes but no peak shift was observed when tilting the samples in χ indicating that the measured cell parameters correspond to the stress-free crystallised SiC layers. For all T_d values, whereas the crystallites of the hexagonal polytype exhibit isotropic shape of nearly 5.6 nm, the mean shape of the 3C-SiC crystallites corresponds to an ellipsoid elongated along the <111> direction and almost isotropic in the other directions. When T_d reaches 600 °C the <111> size value is enlarged from 3 to 5 nm, whereas the size dimension in the perpendicular directions remains almost unchanged (~1.5 nm). The films exhibit also multiple texture

Table 1
Thicknesses as measured by profilometry and refined by the Combined Analysis, compared to the porosity as determined by X-ray reflectivity [9] on two Si nanocrystalline thin films deposited on a-SiO_2 substrates.

Profilometry thickness (nm)	X-ray thickness (nm)	Porosity (%)
1350	711 (50)	26 (3)
1470	1360 (80)	13 (3)

Parentheses indicate the standard deviations on the last digits.

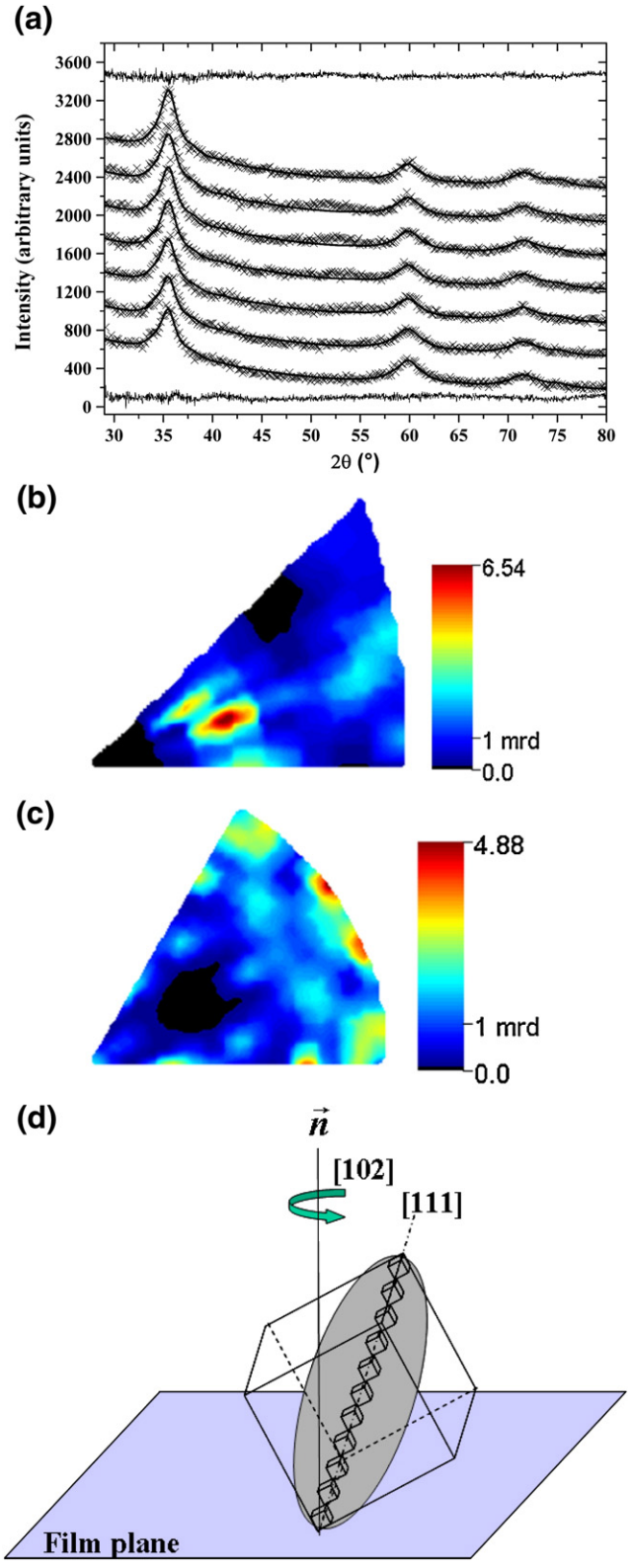

Fig. 3. (a) Experimental (×) and fitted (line) 2θ patterns for selected χ orientations for a nc-SiC film deposited at $T_d = 600$ °C; Bottom pattern: $\chi = 0°$; top pattern: $\chi = 35°$; $\Delta\chi = 5°$. Differences between measured and calculated diagrams are shown for the bottom and top patterns and illustrate the fit quality. Recalculated inverse pole figures for the film normal and for the 3C-SiC (b) and for (c) the 6H-SiC phases (linear density scale, equal area projections). (d) Schematic representation of the growth of a non faulted [111] elongated 3C-SiC crystallite that tends to agglomerate along <102>.

components. For the 3C-SiC polytype a main contribution is observed around the <102> and <11l> texture components with high 1 values (typically 10 or larger) (Fig. 3(b)) whereas the 6H-SiC phase exhibits a main contribution around the <100> direction (Fig. 3(c)). For the two polytypes, the observed texture strengths are weak and the pole figure maxima do not exceed 4 m.r.d.

The [111] elongated 3C-SiC nanocrystals tend to agglomerate in a columnar growth structure (Fig. 3(d)) mainly along the <102> direction, without reaching the pure <111> texture component generally observed for such a zinc-blende structure. The {111} planes tilt with $\alpha = 39°$ from the normal direction of the film has been yet evidenced by Yasui et al. [22], but with only $\alpha = 15.8°$, when the 3C-SiC film exhibits numerous stacking faults. At $T_d = 600$ °C the refined proportion of 6H-SiC is about 33% and increases up to 70% when T_d decreases down to 300 °C (Table 2). In comparison with previous works, the presence of the polytype 6H-SiC at such low temperature is quite surprising and strongly suggests the presence of stacking faults in the 3C-SiC, that cannot be modelled in the actual version of the Maud software. This hypothesis has been asserted by HRTEM studies in which filtered HRTEM images of supposed hexagonal nanocrystals revealed tetrahedron stacking sequences not corresponding to a 6H-SiC sequence but that can be better understood as a highly faulted 3C-SiC phase [10].

Finally, the structure and phase modifications, in terms of crystallization degree, compactness, composition..., on these films have been found to be strongly correlated to the evolution of their optical properties (optical gap and refractive index), that have been optimized for the realization of an nc-SiC/c-SiC heterojunction exhibiting promising properties [10].

3.3. Multiphased Cr^{2+}:ZnSe films: texture, anisotropic crystallite sizes, residual stresses, twin faults and phase analysis

The mid-infrared wavelength region (2–5 μm), which is also often called "molecular fingerprint" region, is of special interest for many important applications such as environmental sensing, infrared countermeasures against heat-seeking missiles, and laser radar. For such applications, robust, compact, solid-state, tunable laser sources operating at room temperature in the mid-IR range are needed leading to a great interest focussed on the transition metal doped II–VI semi-conductors. Among this family, Cr^{2+}:ZnSe is the most widely used host material due to its favourable properties (flexible pumping schemes, impressive output powers, wide tunability in the 2–3.1 μm region and room-temperature operation). With the aim of realizing an electrically pumped compact mid-infrared microlaser, Cr^{2+}:ZnSe films have been grown at room-temperature on various substrates ([100]-GaAs and [100]-Si single crystals and a-SiO_2) by magnetron co-sputtering of a SiO_2 target covered by ZnSe chips and a variable quantity of Cr chips [11,23]. As the production of quality films for fluorescence and stimulated emission studies under optical and electrical excitation is essential, the structural and microstructural properties of theses films must be carefully investigated. We performed X-ray diffraction experiments with $\omega = 13.65°$ corresponding to the Bragg angle of the 111 reflection of cubic ZnSe. Whatever the substrate, the X-ray diagrams exhibit both cubic (C-ZnSe) and

Table 2
Main refined parameters of the 3C-SiC phase and refined proportions of the two polytype phases.

T_d (°C)	$a_{3C\text{-}SiC}$ (Å)	6H-SiC phase (%)	Anisotropic 3C-SiC sizes (Å)			
			[111]	[200]	[220]	[311]
300	4.385 (3)	70 (1)	28 (1)	12 (2)	13 (2)	15 (1)
400	4.380 (1)	66 (1)	34 (2)	12 (1)	16 (2)	15 (2)
500	4.375 (2)	52 (1)	44 (1)	14 (1)	15 (1)	20 (1)
600	4.378 (4)	33 (2)	49 (2)	17 (1)	18 (1)	22 (2)

Parentheses indicate the standard deviations on the last digits.

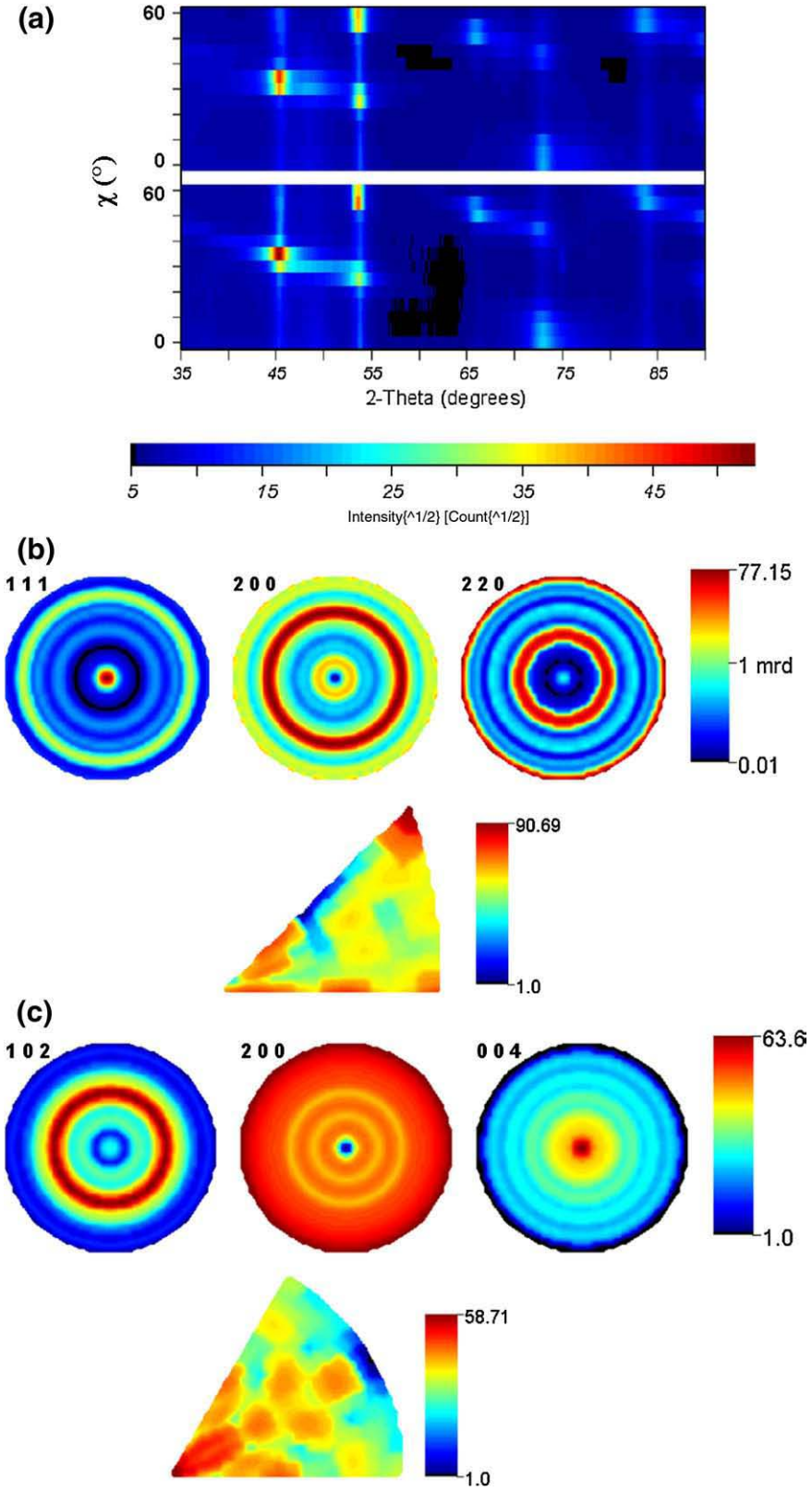

Fig. 4. (a) 2D representation of selected diagrams for a ZnSe film deposited on silica glass at room temperature with a radiofrequency power of 250 W, an Ar gaz pressure of 2 Pa and a Cr quantity on the target of 0.17 g. Bottom diagrams: experiments, top diagrams: refinement. Low indices pole figures and inverse pole figures for the films normal, recalculated from the ODFs for (b) C-ZnSe and (c) H-ZnSe. Equal area projections, logarithm density scale.

hexagonal (H-ZnSe) ZnSe signatures with phase amounts varying with the deposition conditions (radiofrequency power and Cr quantity on the sputtered target). A two dimensional representation of the diffraction diagrams (Fig. 4(a)) clearly demonstrates the achievement of a strong texture of both phases in such films, within reliability factors of $R_w = 25.7\%$ and $R_{exp} = 11.1\%$. The C-ZnSe phase exhibits a strong <111> fibre texture also evidenced in the TEM images (Fig. 5(a)), culminating around 77 m.r.d. (Fig. 4(b)), with some residual

orientations (see inverse pole figure of Fig. 4(b)), while H-ZnSe shows a unique <001> fibre texture with a maximum of nearly 64 m.r.d. (Fig. 4 (c)). At the first growth stage, an amorphous ZnSe thin layer on the [100]-Si and [100]-GaAs substrates (around 3 nm) is observed in the HRTEM images (Fig 5(b)) explaining why the texture is fibre-like independently of the choice of the substrate. The two fibre axes are parallel to the normal of the film plane, as would be expected for a film growth sharing hexagonal planes in a columnar pattern. The C-ZnSe and H-ZnSe phases exhibit anisotropic crystallite sizes (Table 3) also evidenced in the corresponding HRTEM images. Furthermore, both phases show strong residual stresses, as can be seen from the peak shifts with χ in Fig. 4(a). The geometric mean approach allowed to resolve during the combined fit tensile in-plane stresses of several hundreds of MPa in both phases (Table 3), using a biaxial model [24] with $\sigma_{11} = \sigma_{22}$ as imposed by the fibre character of the texture. The residual stresses in H-ZnSe are about twice the ones of C-ZnSe. Such stress levels cannot be achieved by the substrate influence since no heteroepitaxial relationship is observed between films and substrates. The presence of residual stresses was also reported by Rizzo et al. in pure ZnSe sputtered films onto [100]-Si substrates which also exhibited fibre textures, however with no quantitative characterisation neither of the texture nor of the stresses [25]. The authors attributed the stress achievement in their films to the momentum transfer parameter (β) linked to energetic transfers from incident particles sputtered to the growing films. However, in our deposition conditions β as described by the authors should place our film under compressive in-plane stress, contrarily to our observations. These discrepancies could be explained either by a stronger presence of H-ZnSe in our films (our refined value is 45.4 (5)% of H-ZnSe in volume), or by the fact that the texture has to be taken into account in the estimate of in-plane stresses and strains when estimated from out of plane measurements.

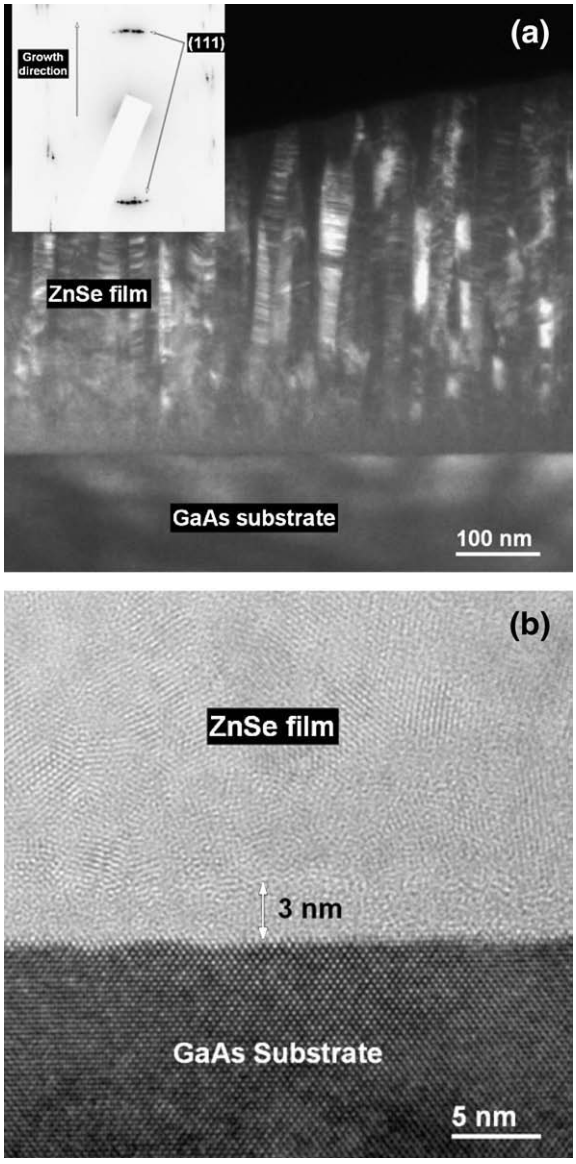

Fig. 5. (a) Bright-field TEM image and its corresponding selected area electron diffraction pattern showing the columnar growth of a Cr^{2+}:ZnSe thins film exhibiting strong <111> fibre texture; (b) HRTEM image showing the amorphous layer invariably present at the interface with the substrate (here GaAs), and explaining why the main texture <111> component is constantly observed for single crystals or amorphous substrates.

Table 3
Refined parameters for the two ZnSe phases (H-ZnSe and C-ZnSe).

Phase	Cell parameters (Å)	In-plane stress (MPa)	Anisotropic sizes (Å)			
			[111]	[100]	[110]	[103]
C-ZnSe	$a = 5.6497$ (3)	263 (14)	112 (1)	117 (5)	85 (1)	–
H-ZnSe	$a = 3.9527$ (6) $c = 6.7154$(8)	436 (25)	–	244 (1)	244 (2)	20 (2)

Single-crystal elastic tensors used in the residual stress calculations are taken from Ref. [23]. Parentheses indicate the standard deviations on the last digits.

Finally, one can observe that our fits are not optimum on this kind of samples. In particular, the anisotropic Popa model cannot account completely for the peak broadening of the H-ZnSe phase. In order to better reproduce our diagrams the incorporation of twin faults appeared necessary (stacking faults did not provide better refinement) in this phase, with a probability of 45.7(6)%. Such twins are also suggested by the bright field TEM image of Fig. 5(a) and would be coherent with the observation of the two strongly linked fibre textures corresponding to the classical scheme of cubic-hexagonal systems, and with the occurrence of large residual stress states. However if the introduction of twin faults in the H-ZnSe phase improves our fits for $2\theta > 35°$, the reproduction of the experimental data for $2\theta < 35°$ is not optimum (not represented here) with still discrepancies especially for the 111-C and 002-H line fits. We could not further improve the fits considering stacking faults (intrisinc or extrinsic), and microstrain incorporation systematically gave rise to insignificant values (typically less than 10^{-4} rms within as large standard deviations or even slightly negative). This underlines that another still unidentified phenomenon is not accounted for in the diagrams. In order to achieve large intensity of the 111-C line, intergrowth between C and H phases could play a rule. However such intergrowth still needs being implemented in the combined algorithm.

The room temperature photoluminescence (PL) spectra under direct excitation (1850 nm) revealed that chromium has been incorporated in the Cr^{2+} active state leading to the mid-infrared emission at about 2200 nm. The determination of the correlation between the structural, microstructural and optical properties of the films, in order to achieve the highest PL intensity in the infrared region, is in progress at the light of the previous recent Combined Analysis results.

4. Conclusion

The X-ray diffraction Combined Analysis characterisation capabilities have been demonstrated for micro- and nano-structured films. The quantitative crystallographic texture determination can be carried out even in films containing two crystalline phases. The ODF of the phases can be used to calculate the residual stresses in the films, even if strong peak overlaps occur due to large peak broadenings. Unit-cell parameters are determined together with phase volume percentages, and crystallite sizes and shapes can be quantitatively estimated. When compared with complementary techniques, films thicknesses deduced from our analysis can be used as a characterisation of porosities in the layers.

In nc-Si films no residual stress is observed and weak fibre textures are stabilised. Elipsoidal crystallite shapes are observed, and a cell-parameter weak expansion is measured due to smaller crystal sizes. Films thicknesses as determined by X-ray diffraction prompt for porosities in the films, when compared to other thickness determinations. In stress-free SiC films, the observed textures are also fibre-like for the two SiC polytypes, with however different fibre axes. Crystallite sizes and shapes are similar to the ones of the Si films. In ZnSe films strong tensile in-plane residual stresses are present which are linked to the strongly developed textures of the cubic and hexagonal phases. The hexagonal ZnSe phase represents around 45% of the volume of the film, and crystallite sizes are anisotropic for both phases.

Throughout this work, the presence of crystallographic textures places the materials between a perfectly randomly oriented powder and a perfect single crystal. This fact is used to provide better determinations of anisotropic parameters.

References

[1] D. Chateigner, In: D. Chateigner (Ed.), Combined analysis: structure – texture – microstructure – phase – stresses – reflectivity analysis by X-ray and neutron scattering, ISTE Publishers, London, to appear march 2009, p. 300; partial proofs at http://www.ecole.ensicaen.fr/~chateign/texture/combined.pdf.
[2] L. Lutterotti, H.-R. Wenk, S. Matthies, in: J.A. Szpunar (Ed.), Textures of Materials, vol. 2, NRC Research Press, Ottawa, 1999, p. 1599.
[3] H.M. Rietveld, J. Appl. Crystallogr. 2 (1969) 65.
[4] S. Matthies, G.W. Vinel, Phys. Status Solidi B 112 (1982) K111.
[5] N.C. Popa, J. Appl. Crystallogr. 31 (1998) 176.
[6] Matthies Humbert, Appl. Crystallogr. 28 (1995) 254.
[7] J. Ricote, D. Chateigner, M. Morales, M.L. Calzada, C. Wiemer, Thin Solid Films 450 (2004) 128.
[8] J. Ricote, M. Morales, M.L. Calzada, Mat. Sci. Forum 408–412 (2002) 1543.
[9] M. Morales, Leconte, R. Rizk, D. Chateigner, J. Appl. Phys. 97 (2004) 034307.
[10] H. Colder, R. Rizk, M. Morales, P. Marie, J. Vicens, J. Appl. Phys. 98 (2005) 024313.
[11] N. Vivet, M. Morales, M. Levalois, J.L. Doualan, R. Moncorgé, Appl. Phys. Lett. 90 (2007) 181915.
[12] 19th International Conference on Amorphous and Microcrystalline Semiconductors, (Nice, France, August 2001), J. Non-Cryst. Solids 299–302 (2002).
[13] Y. Feng, M. Zhu, F. Liu, J. Liu, H. Han, Y. Han, Thin Solid Films 395 (2001) 213.
[14] E. Vallat-Sauvain, U. Kroll, J. Meier, A. Shah, J. Appl. Phys. 87 (6) (2000) 3137.
[15] U. Kroll, J. Meir, P. Torres, J. Pohl, A. Shah, J. Non-Cryst. Solids 69 (1998) 227.
[16] L. Houben, M. Luysberg, R. Carius, Phys. Rev. B 67 (2003) 045312.
[17] J.J. Heizmann, C. Laruelle, J. Appl. Crystallogr. 19 (1986) 467.
[18] S. Matthies, G.W. Vinel, K. Helming, in: S. Matthies (Ed.), Standard distributions in texture analysis, vol. 1, Akademie-Verlag, Berlin, 1987, p. 449.
[19] W.A. Dollase, J. Appl. Crystallogr. 19 (1986) 267.
[20] F.K. Lotgering, J. Inorg. Nucl. Chem. 9 (1959) 113.
[21] P. Bergman, E. Jantzén (Eds.), Silicon Carbide and Related Materials, Mater. Sci. Forum, vol. 433–436, Trans Tech Publications, Switzerland, 2003.
[22] K. Yasui, M. Hashiba, T. Akahane, Appl. Surf. Sci. 216 (2003) 580.
[23] N. Vivet, M. Morales, M. Levalois, X. Portier, J.L. Doualan, Mater. Sci. Eng. B 146 (2008) 236.
[24] R.A. Mayanovi, R.J. Sladek, U. Debska, Phys. Rev. B 38 (2) (1988) 1311.
[25] A. Rizzo, M.A. Tagliente, L. Caneve, S. Scaglione, Thin Solid Films 368 (2000) 8.